Numerical Simulation of Warm-Air Drying of Mexican Softwood

Sadoth Sandoval- Torres [1], Emilio Hernández-Bautista [*1], and Juan Rodríguez-Ramírez [1], Artemio Carrillo Parra[2]
[1]Instituto Politécnico Nacional. CIIDIR Unidad Oaxaca, [2]Instituto Politécnico Nacional. CIIDIR Unidad Oaxaca [3]Instituto Politécnico Nacional. CIIDIR Unidad Oaxaca
* 71230, ssandovalt@ipn.mx
[2]Facultad de Ciencias Forestales, Universidad Autónoma de Nuevo León, Linares, N.L. México.

Abstract: In this work, the numerical simulation of Mexican softwood (*Pinus pesudostrobus*) drying is presented by solving a physics-based model. The model was developed by considering the heat and mass transport and the representative elementary volume, which involves the solid, liquid and gas phases. We solved a system of partial differential equations by numerical factorization in COMSOL multiphysics 3.4©. Three primary variables were solved: the moisture content, the temperature, and the dry-air density. The warm-air drying of Mexican softwood was simulated on a one-dimensional basis. The liquid water, water vapor pressure, dry-air density and moisture evolution at different depth of wood thickness display a good reliability of our numerical simulation.

Keywords: Warm-air drying, *Pinus pseudostrobus* wood, physics-based model, numerical simulation.

1. Introduction

The evacuation of water in biological materials like wood is a very complex phenomenon, since it involves coupled mechanisms that occurring simultaneously during drying [1]. Wood is extremely no homogeneous, and its structural and chemical variability is reflected in its transport properties such as permeability, capillary behavior, thermal conductivity, and the bound water diffusion coefficient [2]. There are four key relationships in the structure of wood cell walls: (i) aggregation of cellulose, lignin, and hemicelluloses molecules to form larger structures; (ii) arrangement of these structures to conform a multilayered cell wall; (iii) different concentrations of cellulose, hemicelluloses, and lignin within the cell wall and the intercellular region; and (iv) specialization of cell walls, such as interconnecting pits. Since the different polymers that make wood each have different sorption isotherms, and thermal conductivity, wood is in fact a composite material where the overall behavior is a result of the properties of the individual components and their arrangement in wood structure [3]. Then, transport phenomena in wood can be a very difficult task if we consider this arrangement. To overcome this difficulty we employ the average concept.

Water in wood can exist as either absorbed (free water) in the cell lumens and intercellular spaces or as adsorbed (bound water) within the cell walls. When wood dries, liquid water first evaporates from the lumens and intercellular spaces. Two regions exist in wood, the first one called the capillary region and the second one the hygroscopic. Both regions are limited by the fiber saturation point of wood. The fiber saturation point (FSP) is defined as the moisture content at which all the absorbed water has been removed but at which the cell walls are still fully saturated. This occurs at a moisture content of 25 to 35%. In softwoods, it is adequate to presume the fiber saturation point to be 30% moisture content [4, 5].

Moisture flow in wood is a very complex phenomena, since different wood-water relations exist. The flow paths through softwoods are showed in Figure (1).

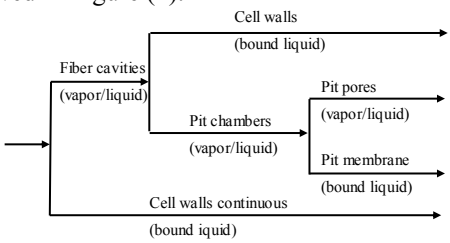

Figure 1. Flow paths through softwoods [2].

During drying, at the same time liquid water is being removed from the capillaries, it is replaced by air and water vapor. This gas flow (air+water vapor) in porous media is transported through the cell wall by adsorption, diffusion, and desorption (Figure 2).

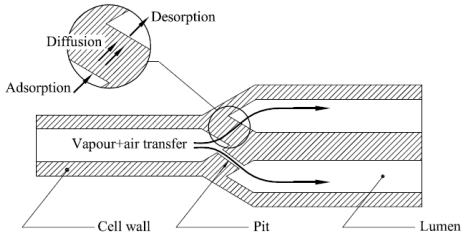

Figure 2. Water vapor and air transport in wood [6].

During drying, the evaporative front divides the board into two regions: a wet region and a much drier region in the outer wedge. In the drier region, moisture is assumed to exists as both bound and vapor water. The bound water is removed from the solid matrix by desorption and subsequently transported by diffusion. Bound water will be in local thermodynamic equilibrium with the water vapor at the local temperature. The drying process stops when the equilibrium moisture content is reached.

In the past years, several models have been proposed. The most advanced models are called "physics-based models". These models take into account the thermodynamic fundamentals of transfers in porous media, and consider the contribution of each phase [7]. Some phenomenological models has been modified to offer more efficient solutions [8], these models involves coupled balances by considering the representative average volume concept (REV).

Several publications dealing with wood drying exist in literature. Many oriented to European woods, as pine (*Pinus maritime*) and oak (*Quercus pedonculae*) [9,10,11,12], nevertheless, the lack of drying models for Mexican softwoods (endemic species) limits the improving of this operation, since one of the handicaps of the Mexican forest industry is the poor technological development [12]. Modeling the drying process will provide useful information to optimize the drying operation. The present work is a first attempt.

The aim of this work was to develop and solve on a one-dimensional basis a physics-based model to simulate drying kinetics and moisture distribution during a warm-air convective drying of Mexican softwood (*Pinus pseudotrobus*).

1.1 Materials and methods

Drying trials were carried out in a dryer tunnel. A univariate statistical design was used where temperature was controlled at 4 levels. The air drying temperature was controlled at 50 60 70 and 80°C. The air velocity was constant in all trials (2.5 m/s), and the relative humidity was not controlled but it was measured. The drying agent (humid air) was heated by two electrical resistances of 20Ω, (2.4 kW) and controlled by a PID system. Both the air temperature and the relative humidity were measured by a Vaisala sensor. Two thermocouples were installed inside the wood, the first one near from the surface and the second one in the middle (Figure 3). The weight of the sample was measured by a load cell (COLE-PARMER, range 0-11.34 kg, 0.1% accuracy). All data are logged by using a data acquisition system (Texas National Instruments) through the LabVIEW software.

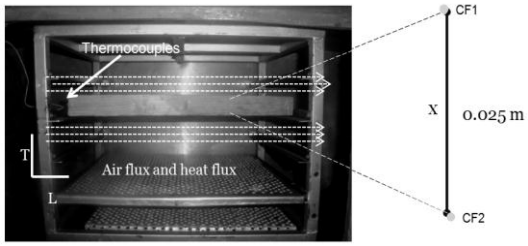

Figure 3. Experimental setup in the drying tunnel and geometry.

Fresh wood boards were taken at random from the sawmill "Pueblos Mancomunados de la sierra Norte", located in the community of Macuilxochitl Artigas Carranza, near from Oaxaca city -Mexico. The samples were 25 cm long, 15 cm wide, and 2.54 cm thickness. The fresh boards were immediately sprayed by using a disperser and covered with a waterproof plastic. The wood samples were immediately stored at 0°C in the refrigerator to prevent degradation. For each experiment two samples of fresh wood were used. The edges were sealed with silicone in order to ensure a one-directional (1-D) transport. Each trial takes approximately 70 hours. All drying conditions were duplicated.

2. Mathematical model

A mathematical formulation was numerically solved by taking into account a multiphase perspective [7, 15]. We assumed the moisture transport is done mainly in the thickness direction (1D), and then the model's geometry is represented in COMSOL by a straight line (Fig.

3), where the line represents the thickness of wood.

The three primary variables to solve were: the moisture content (W); the intrinsic density of air (ρ_a) and the temperature (T).

The moisture transfer (equation 1) is a more elaborate version of the diffusive model; it considers the transport of liquid water, vapor water and bound water. The separation of phases and the constitutive relations include the contribution of each of the phases. The flow of free water is assumed to follow a particular behavior described by Darcy's law; therefore the mass average velocity is given by equation 2. Capillary pressure causes the liquid to move towards the drying surface. Several works has shown the gravity term is very small and therefore negligible [16, 17].

$$\frac{\partial W}{\partial t} = -\nabla \cdot \left\{ \frac{1}{\rho_s} \left(\overline{\rho}_l \overline{\mathbf{v}}_l^l + \overline{\rho}_v \overline{\mathbf{v}}_v^g + J_b \right) \right\} \quad (1)$$

$$\rho_l \mathbf{v}_l = \rho_l \frac{\mathbf{Kk}_{rl}}{\mu_l} \nabla \cdot P_c - \rho_l \frac{\mathbf{Kk}_{rl}}{\mu_l} \nabla \cdot P_g^g \quad (2)$$

The transfer of water vapor and dry air can be described by the combination of Fick's and Darcy's law. Therefore we can represent the transport of gaseous phase (water vapor and dry-air) by the equations 1, 3, 4 and 5. The flow of dry air is similar to water vapor expression, which has two terms (equation 4), the pressure gradients and the concentration gradients.

The equation to explain dry-air mobility (Equation 5) represents the convective flow of gas-phase that result from a total gaseous pressure. It considers the contribution of the pressure gradients which are present in the thickness of wood. The contribution of dry-air can be computed since we consider the Raoult's law for the gaseous mixture.

$$\frac{\partial}{\partial t}\left(\overline{\rho}_a\right) + \nabla \cdot \left(\overline{\rho}_a^g \overline{\mathbf{v}}_a\right) = 0 \quad (3)$$

$$\overline{\rho}_v^g \overline{\mathbf{v}}_v = -\overline{\rho}_v^g \frac{\mathbf{Kk}_{rg}}{\mu_g} \cdot \nabla \overline{P}_g^g - \overline{\rho}_g^g \mathbf{D}_{eff} \nabla \left(\frac{\overline{\rho}_v^g}{\overline{\rho}_g^g} \right) \quad (4)$$

$$\overline{\rho}_a^g \overline{\mathbf{v}}_a = -\overline{\rho}_a^g \frac{\mathbf{Kk}_{rg}}{\mu_g} \cdot \nabla \overline{P}_g^g - \overline{\rho}_g^g \mathbf{D}_{eff} \nabla \left(\frac{\overline{\rho}_a^g}{\overline{\rho}_g^g} \right) \quad (5)$$

The transport mechanism of bound water is described by equation 6. This expression takes into account two mechanisms; the bound water content gradients (Dufour effect) and temperature gradients (Soret effect).

$$J_b = -\rho_s \mathbf{D}_{\mathbf{b}} \cdot \nabla W_b - \rho_s \underset{bt}{D} \nabla T \quad (6)$$

The water activity is written as relative humidity (%RH). At the FSP point %RH is unity, and therefore no vapor-pressure gradients are possible above the FSP-saturation point. The model considers diffusion occurs due to bound water transport and variations in vapor partial pressure since them depend on both temperature and moisture content. Moreover, gas-phase convective transport occurs due to the development of total pressure gradients inside the board.

Stamm [18] has suggested that the relative vapor pressure, or relative humidity, at FSP saturation is about 0.995, whereas Skaar [19] takes a value for the relative humidity of 0.99 at the FSP point. This depression of the relative humidity at FSP saturation is presumed to be caused by both condensation of water at the lumen ends and the tiny micropores and/or cavities in the cell wall. In this work we have used the isotherms published in Rodriguez et al [20], which are specifically for Mexican softwood.

Equation 7 represents the energy balance in wood. It considers heat conduction and the energy contribution of each phase, as well as the enthalpy changes due to the phase change.

$$\rho C_p \frac{\partial T}{\partial t} + \Delta h_{vap} \overline{m}_{lv} + \Delta h_{sorp} \overline{m}_{bv} + \left(C_{pl} \rho_l \mathbf{v}_l + C_{pb} \rho_b \mathbf{v}_b + C_{pv} \rho_v \mathbf{v}_v + C_{pa} \rho_a \mathbf{v}_a \right) \cdot \nabla T = \nabla \left(\lambda \nabla T \right) \quad (7)$$

The surface fluxes are calculated using the heat- and mass-transfer coefficients and the corresponding potentials. Continuity of moisture transfer must occur at the board surface. As mentioned above, Figure 3 shows model's geometry. There are two boundary conditions CF1 and CF2, they are initially considered at the same temperature, these boundaries conditions represent the experimental conditions affecting the wood surface.

Equation 8 represents the outward flux of water vapor leaving the material. This is the boundary condition for the moisture content conservation equation.

$$\mathbf{J}_{\mathbf{w}} \cdot \hat{\mathbf{n}} = \overline{\mathbf{m}}_{\mathbf{lv}} = k_m c M_v \ln\left(\frac{1 - x_{v_\infty}}{1 - x_v} \right) \quad (8)$$

To solve the dry-air equation, a Neumann boundary condition is applied, since it is a flux.

For the energy equation, since the heat over the surface is removed by the airflow, the equation 9 takes into account the convective heat transfer and the energy needed to remove moisture. To

consider the real situation during drying, we have computed the coefficients of heat and mass transfer from experimental data.

$$\mathbf{J_e}\cdot\hat{\mathbf{n}} = \mathbf{q} + \Delta h_v \overline{\mathbf{m}}_{lv} = h(T - T_\infty) + \Delta h_v k_m c M_v \ln\left(\frac{1 - x_{v_\infty}}{1 - x_v}\right) \quad 9$$

To simulate the drying kinetics was necessary to have the thermo-physical properties for this Mexican softwood (*Pinus pseudostrobus*). This conifer wood has been poorly studied. However, we have used the thermo-physical properties of similar conifers (similar in density).

3. Implementation in COMSOL multiphysics.

The model has been solved by using the nonsymmetric-pattern multifrontal method and direct LU factorization of the sparse matrix. It employs the COLAMD (column approximate minimum degree ordering) and AMD approximate minimum degree preordering algorithms to permute the columns so that the fill-in is minimized. The model has been implemented in the commercial software COMSOL Multiphysics 3.4a.

To solve the highly non-linear equations system, the mesh used consists of 125 elements. A relative and absolute tolerance of 0.1 and 0.01 respectively. Relative tolerance needs to be scalar, and is used to control al unknown variables. Absolute tolerance allows to single out individual variables. The system of equations was solved using a computer with processor Intel Core Duo 1.83 GHz.

3 Results

We considered constant air-flow temperature at 60°C, an initial drying temperature of 25°C and an initial moisture content of wood of 96% (wet basis).

In Figure 4, the drying kinetics were simulated and compared versus both the drying characteristic curve method and experimental data. The characteristic curve method was published previously [14]. Figure 4 includes an axis on the right side to plot the temperature profiles in both the center and on the surface of the boards.

At high moisture contents (at the beginning), the capillary flow is most important. Therefore, for *Pinus pseudostrobus* (conifer wood), water-vapor diffusion is likely to be inconsiderable above the fiber-saturation point because the water activity, which is the driving force for water-vapor transport above the fiber-saturation point. In the first hours of drying, capillary pressure is the driving force of transport. A deviation near from the FSP can be explained by a highly variation of capillary pressure for woods. Furthermore, the FSP was 0.3, which is a value proposed for conifers but it could be different.

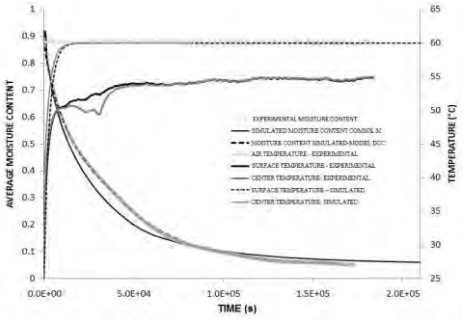

Figure 4. Drying kinetics and average temperature evolution.

According to Nijdam [5], the surface temperature often approaches an asymptotic value well below the external air temperature when drying sapwood under high-temperature conditions, in our experiments, we have applied temperate temperature, and it can be observed the asymptotic value is never reached. To improve the temperature evolution it should be important to consider a more appropriate thermal conductivity for *Pinus pseudostrobus*.

Figure 5 shows the moisture distribution within the thickness of the wood and its evolution in intervals of 1000 secs. While liquid water is removed, it is replaced by the gaseous phase.

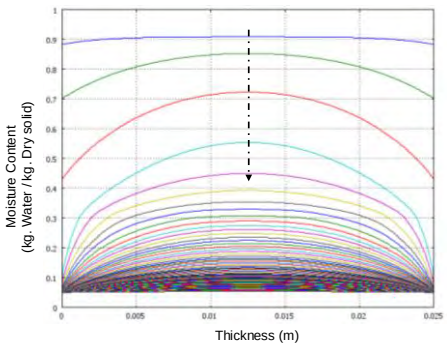

Figure 5. Moisture distribution through the thickness of wood every 1e3 secs.

A fluctuation in the parable of moisture content is due to the phase transition, because of the capillary phase finish and hygroscopic phase begins. This fluctuation mainly depends on both the relative permeability function and the capillary pressure terms, whose influence directly affects the liquid water transport. Mathematically, the saturation term softens the parables with squared functions.

In figure 7 and 8, we show the water vapor pressures and the dry-air density inside wood respectively.

Our model assumes that the relative humidity of the gas at the fiber-saturation point is unity, and therefore no vapor-pressure gradients are possible above the fiber-saturation point. For this reason, the water activity expression is considered only below the fiber-saturation point (FSP). We recall that the gas mixture is a combination of water vapor and dry air, and this is described by Dalton's law which establishes the pressure of a mixture of non-reactive gases, is equal to the sum of each of them. The solution of water vapor expression is a parabolic function. The vapor pressure evolution indicates this behavior during drying.

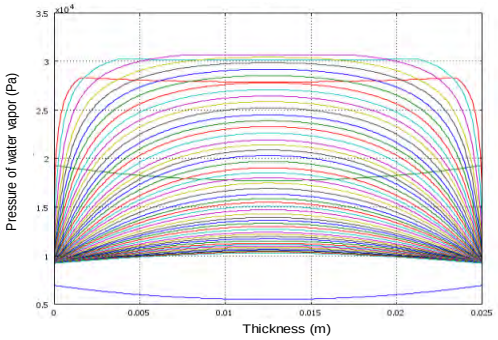

Figure 6. Vapor pressure distribution through the thickness of wood every 1e3 secs.

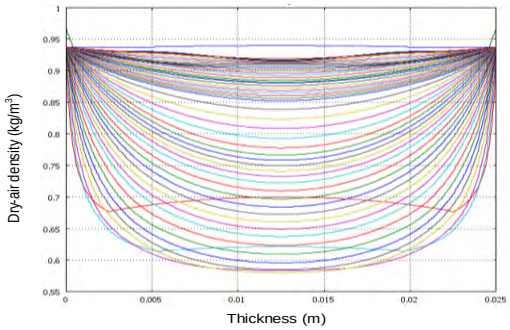

Figure 7. Dry air density distribution through the thickness of wood every 4e3 secs.

It would be interesting to see the moisture losses at different depths of the board. In Figure 8 we present these data. It shows how moisture in wood surface reaches equilibrium firstly. Is convenient to say in this work we have used sapwood only. It is well known about the differences between sapwood and heartwood drying. The evaporative front recedes promptly in heartwood drying because there are no significant liquid flows in the wet region to maintain the position of the evaporative plane neighboring the surface. Moisture losses at different depths of wood are well simulated. Some regions (layers of wood at the surface) reach equilibrium moisture content faster, which is coherent with drying physics.

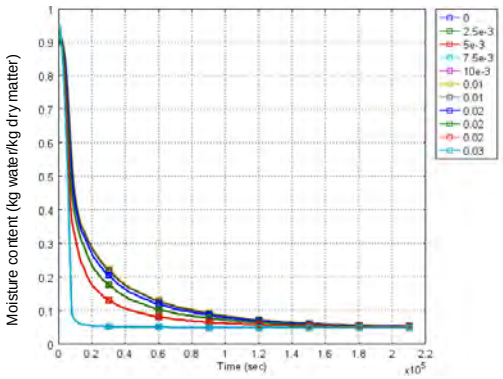

Figure 8. Moisture content evolution at different depths (each 2,5mm) within the board.

The evaporative front recedes and the velocity with which it recedes is well observed. Figure 8 show the moisture distribution develops different drying rates, and at the surface, moisture decrease strongly.

4. Conclusions

Drying kinetics, moisture distribution inside wood and gas transport was correctly simulated. Many of the transport properties required by the model correspond to similar softwood species, so the variations in the theoretical kinetics could be diminished if their thermo-physical properties were experimentally obtained.

The results demonstrate the importance of accounting for thermo-physical properties variations. For example, the thermal conductivity of wood could change by the particular chemistry of Mexican softwood.

At the end of drying, the voids spaces are filled with dry air, so thermal conductivity changes by this fact too. Nevertheless, in this work thermal conductivity is strictly a function of moisture content.

To enhance the phenomenological model the thermal and transport properties must be experimentally calculated for this wood specie.

Nevertheless, the numerical results describe correctly the drying behavior of *Pinus psedostrobus* wood, and moisture distribution. The model displays a strong reliance of the physical properties of wood. This is the first time a drying simulation for Mexican softwood is accomplished. COMSOL multiphysics is a well adapted software to simulate this kind of processes.

5. References

1. P. Perré, I. W Turner, A Dual-Scale Model for Describing Drier and Porous Medium Interactions. *AIChE Journal*, **52**(2006), 3109-3117.

2. J. F. Siau. Transport Processes in Wood*: Springer Series in Wood Science*. (1984) pp. 245

3. A.G. McDonald, Constituents in wood. In: Encyclopedia of Materials: Science and Technology. *Elsevier Science* (2001) pp. 9612-9616

4. J.C.F Walker, *Water in wood. In: Primary Wood Processing*, 606, Netherlands (2010).

5. J.J. Nijdam, T.A.G. Langrish, R.B. Keey, A high-temperature drying model for softwood timber. *Chemical Engineering Science* **55**(2000) 3585-3598.

6. K. Krabbenhøft,. Moisture Transport in Wood. A Study of Physical--Mathematical Models and their Numerical Implementation. *Technical University of Denmark, Denmark*, (2003)

7. S. Whitaker, Simultaneous heat, mass and momentum transfer in porous media: a theory of drying. *Advances in Heat Transfer*, **13**(1977), 119–203.

8. P. Perré, How to get a relevant material model for wood drying simulation? *Advances in drying of wood* (1999).

9. M. Fernandez, J. Howell, Convective drying model of southern pine. *Drying technology*, **15**(1997), 2343-2375.

10. S. Raji, Y. Jannot, P. Lagière, J. Puiggali, Thermophysical characterization of a laminated solid-wood pine wall. *Construction and Building Materials*, **23**(2009) 3189–3195.

11. I. Turner, J. Puiggali, W. Jomaa, A numerical investigation of combined microwave and convective drying of a hygroscopic porous material: A study based on pine wood. *Trans IChemE*, **76**(1998) 193-209.

12. P. Perré, I. Turner, Transpore : A generic heat and mass transfer computational model for understanding and visualising the drying of porous media. *Drying Technology*, **17**(1999), 1273-1289.

13. H. Forster, A. René, A. Argüelles, N. Aguilar, S. Kaatz, Opciones Y Barreras De Mercado Para Madera Aserrada De Michoacán, Oaxaca, Guerrero, Campeche Y Quintana Roo, Mexico. *Report to Forest Trends. Mexico* (2004)

14. E. Hernández-Bautista, S. Sandoval-Torres, J. Rodríguez-Ramírez, O. A. Velasco-Cruz. Modelización del secado de madera de Pinus pseudostrobus utilizando el método de la curva característica. *Bois et forêts des tropiques*, 306 (2010).

15. P. Perré, I. W. Turner, A Dual-Scale Model for Describing Drier and Porous Medium Interactions. *AIChE Journal*, **52**(2001), 3109-3117.

16. O. Plumb, M. Prat, Microscopic model for the study of drying of capillary porous media. *Drying '92*, (1992) 397-406.

17. I. Turner, P. Rousset, R. Rémond, P. Perré, An experimental and theoretical investigation of the thermal treatment of wood (Fagus sylvatica L.) in the range 200–260 C. *International Journal of Heat and Mass Transfer*, **53** (2010) 715–725.

18. A.J. Stamm, Review of nine methods for determining the fiber saturatioin points of wood and wood products. *Wood Science* **4**(1971) 114-128.

19. C. Skaar, Wood-Water Relations, 632, Berlin(1988).
20. J. Rodriguez-Ramirez, S. Sandoval-Torres, L. Mendez-Lagunas, A.C. Parra, Experimental determination and modeling of equilibrium moisture content from the sapwood of Mexican pine (Pinus pseudostrobus Lindl.). *Forestry Studies in China*, **13**(2011), 285-289.
21. M. Fuentes-Salinas, Estimación del punto de saturación de la fibra (psf) de las maderas. *Revista Chapingo Serie Ciencia Forestales y del Ambiente*, **6**(2000), 79-81.
22. J. M. Hernández, J. R. Puiggali. Simulation of drying of coniferous wood using varius processes. *International Chemical Engineering*, **34**(1994), 339-350.
23. W. Kang, W.Y. Chung, Liquid water diffusivity of wood from the capillary pressure–moisture relation. *The Japan Wood Research Society*, **55** (2009), 91-99.
24. M. H. Colakoglium, Determination of Change in Moisture Ratios of Some Woods during Air-Drying by Finite Element Analysis. *Journal of Applied Sciences* **9**(2009), 4091-4094.
25. R. Baronasa, F. Ivanauskasa, I. Juodeikienėc, and A. Kajalavičiusc, Modelling of Moisture Movement in Wood during Outdoor Storage. Nonlinear Analysis: *Modelling and Control*, **6**(2001).
26. K. Wook, W.Y. Chung, C.D. Eom, H. Yeo, x Some considerations in heterogeneous nonisothermal transport models for wood: a numerical study. *The Japan Wood Research Society* **54**(1977), 267–277.
27. S. Sandoval-Torres, J. Rodríguez-Ramírez, L. Mendez-Lagunas, A. Carrillo-Parra, Experimental Determination and Modelling of Equilibrium Moisture Content from the Sapwood of Mexican Pine (Pinus Pseudostrobus). *Forestry Studies in China* (2011).

6. Acknowledgements

To Instituto Politécnico Nacional, CIIDIR Oaxaca. México.
Thank you very much to COFAA-IPN.